Supplementary Information

Evidence of Ferrimagnetism in Fe_3GaTe_2 via Neutron Diffraction Studies

Mario Lopez[1], Peng Yan[2], Peter Y. Zavalij[1], Anahita Javadi[1], Ivan da Silva[3], Zhongxuan Wang[1], Shenqiang Ren[1], Joseph W. Bennett[2], Efrain E. Rdoriguez[1]

[1] University of Maryland, College Park; 8051 Regents Dr. College Park, MD 20742

[2] University of Maryland, Baltimore County; Baltimore, MD 21250

[3] ISIS Neutron and Muon Source; STFC, Rutherford Appleton Laboratory, Chilton, Oxfordshire OX11 0QX, U.K.

mlopez95@umd.edu; efrain@umd.edu

Table of Contents

I. Experimental Methods

Synthesis of Fe_3GaTe_2 Single Crystal:

Single crystals were made from a self-flux synthesis reported in Zhang et.al [1]. Fe (Alfa Aesar, 99.5%), Ga (Thermofisher, 99.99%), Te (Sigma-Aldrich, 99.8%) were mixed in a 1:1:2 ratio inside a glove box and placed inside a quartz ampoule. The ampoule was heated to 1000 °C in 3 hours. Next, it was dwelled at 1000 °C for 24 hours. Afterwards the sample was quenched to 880 °C within 1 hour followed by a slow cool to 780 °C at a rate of 1 °C/Hr. Then, the sample was quenched. A large molten, metallic rock-like substance was extracted from the ampoule. This metallic rock was observed to be magnetic in ambient conditions, which is a sign that FGaT has grown within the rock sample. However, it is mixed in with the rest of rock which mostly is comprised of Ga_2Te_3. To isolate Fe_3GaTe_2 from the self-flux rock, a razor blade was carefully applied to scrape some flakes on the more metallic flat surfaces on the rock. These flakes were collected and a single crystal for Fe_3GaTe_2 was measured for SCXRD.

Synthesis of Polycrystalline Fe_3GaTe_2:

Powder Fe_3GaTe_2 was synthesized as follows: GaTe was synthesized in an ampoule prepared in an Ar-filled glovebox at 900°C for 3 days. The ampoule had one part Ga (Thermofisher, 99.99%) and one part Te (Sigma-Aldrich, 99.8%) with an additional 0.1-0.3% of Ga was added to ensure the production of GaTe instead of Ga_2Te_3 based on the binary phase diagram. Afterwards, inside an Ar filled glovebox, one part of GaTe, one part Te and three parts Fe (Alfa Aesar, 99.5%) was mixed a mortar and pestle and placed in an ampoule. The reaction was heated to 700 °C with 1-2 hours and welled at that temperature for 6 days. The ampoule was then allowed to naturally cool in the furnace before extraction.

Single Crystal X-ray Diffraction and Refinement:

Suitable single crystals of $Fe_{2.97(2)}Ga_{0.93(1)}Te_2$ were selected and measured on a Bruker D8Venture with Photon III diffractometer with a Mo source [2]. The crystal was kept at 250 K during data collection. The integral intensity was corrected for absorption using SADABS software [3] by using an integration method. The resulting minimum and maximum transmission are 0.065 and 0.808 respectively. The structure was solved with the ShelXT [4] program and refined with the ShelXL program using least-square minimization [5]. Zero restraints were used in the refinement.

Powder X-ray Diffraction and Refinement:

X-ray diffraction was performed on a Bruker D8 Advance diffractometer with a Cu K_α source at ambient conditions. For the Rietveld refinement, GSAS-II [6] refinement software was used. CIF file used for the Fe_3GaTe_2 phase was from our model derived from the SCXRD experiment. CIF file used for FeTe was obtained from the ICSD (Coll. Code: 180602). For the refinement only one restraint used was forcing the U_{iso} thermal parameters between Fe1 and Fe3 to be equivalent to each other.

Neutron Powder Diffraction and Refinement

Neutron Powder diffraction was accomplished at the GEM Instrument at the ISIS Neutron and Muon Source. Data was collected through six banks ranging from 0.4 Å to 25 Å. Here two sample environments were used. In the cryo-environment setting, our samples were measured at 1.5 K, 50 K, 100 K, and 150 K. Each run was measured for 3 hours. For the ambient environment the low temperature furnace was used to measure FGaT from 298 K to 473 K in 25 K increments. Once again, each run was measured for 3 hours. The sample mass for this experiment was about 6 grams. Collected data was analyzed with GSAS-II refinement software. A combined refinement of Bank 2, 4, and 6 was used as the basis of our Rietveld refinement. For this refinement the only constraint applied was to make the U_{iso} of both Fe1 and Fe3 equivalent.

Computational Methodology:

First-principles calculations were performed using the open-source software package QUANTUM ESPRESSO [7], based on periodic plane-wave density functional theory (DFT) [8–10]. The Perdew–Burke–Ernzerhof (PBE) [11] generalized gradient approximation (GGA) was adopted, along with the van der Waals (vdW) interaction correction in Grimme's DFT-D2 method [12] (with a global scaling factor $S_6 = 0.5$) for all calculations. GBRV [13] ultrasoft pseudopotentials were used to describe all atoms, with a plane-wave basis cutoff of 40 Ry for the primitive bulk structures. Lattice optimization calculations were performed using a 6 × 6 × 6 Monkhorst–Pack k-point grid [14]. All self-consistent calculations were carried out with a convergence criterion of 1×10^{-7} eV and a force tolerance of 1–5 meV/Å per atom. The optimized lattices were then used for band structure and projected density of states (PDOS) calculations, employing a 10 × 10 × 10 Monkhorst–Pack k-point grid [14].

II. Single Crystal X-ray Diffraction Results

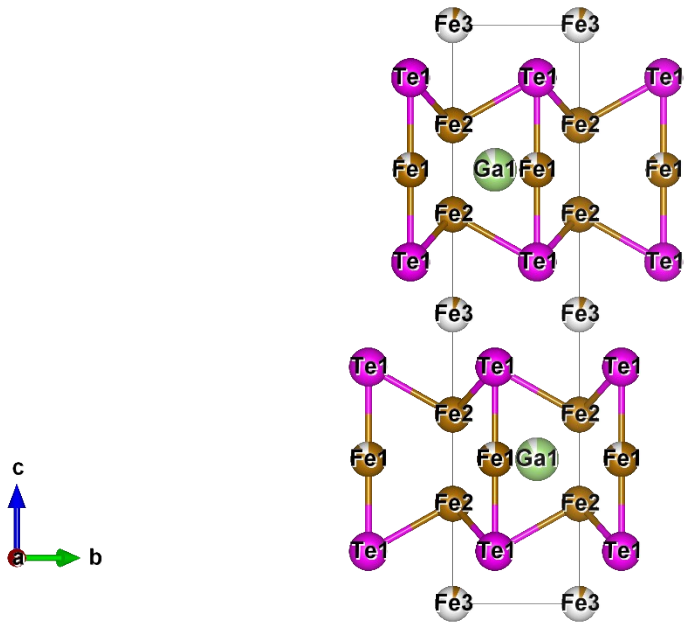

Figure S1. FGaT crystal structure with atoms labeled.

Table S1. Complete crystal data and structure refinement for $Fe_{2.98}Ga_{0.93}Te_2$

Parameter	Value
Empirical Formula	$Fe_{2.97(2)}Ga_{0.93(1)}Te_2$
Formula Weight / g/mol	485.84
Temperature / K	250(2)
Crystal System	Hexagonal
Space Group	$P6_3/mmc$
***a* / Å**	4.0723(3)
***b* / Å**	4.0723(3)
***c* / Å**	16.0928(15)
α / °	90
β / °	90
γ / °	120
Volume / Å^3	231.13(4)
Z	2
ρ_{calc} / g/cm^3	6.981
μ / mm^{-1}	26.658
F(000)	420.0
Crystal size / mm^3	0.21 × 0.18 × 0.01

Radiation	MoKα (λ = 0.71073)
2Θ range for data collection/°	5.062 to 59.916
Index ranges	$-5 \leq h \leq 5$, $-5 \leq k \leq 4$, $-22 \leq l \leq 22$
Reflections collected	2096
Independent reflections	162 [R_{int} = 0.0318, R_{sigma} = 0.0170]
Data/restraints/parameters	162/0/14
Goodness-of-fit on F^2	1.200
Final R indexes [I>=2σ (I)]	R_1 = 0.0282, wR_2 = 0.0681
Final R indexes [all data]	R_1 = 0.0319, wR_2 = 0.0694
Largest diff. peak/hole / e $Å^{-3}$	1.99/-1.04

Table S2. Fractional Atomic Coordinates with Wycoff site labels, Occupancies, and Equivalent Isotropic Displacement Parameters ($Å^2 \times 10^3$) for single crystal FGaT. U_{eq} is defined as 1/3 of the trace of the orthogonalized U_{IJ} tensor.

Atom	*x*	*y*	*z*	U(eq)	Occ.
Fe1 (2*d*)	0.3333	0.6667	0.75	10.1(8)	0.903(14)
Fe2 (4*e*)	0	0	0.3270(1)	10.7(4)	1
Fe3 (2*a*)	0	0	0.5	10.7(4)	0.070(8)
Ga1 (2*c*)	0.3333	0.6667	0.25	18.7(8)	0.925(12)
Te1 (4*f*)	0.3333	0.6667	0.5907(1)	12.2(3)	1

Table S3. Anisotropic Displacement Parameters ($Å^2 \times 10^3$) single crystal diffraction of FGaT

Atom	U_{11}	U_{22}	U_{33}	U_{23}	U_{13}	U_{12}
Fe1	8.1(10)	8.1(10)	14.1(12)	0	0	4.1(5)
Fe2	8.6(5)	8.6(5)	15.0(7)	0	0	4.3(3)
Fe3	8.6(5)	8.6(5)	15.0(7)	0	0	4.3(3)
Ga1	18.5(10)	18.5(10)	19.0(11)	0	0	9.3(5)
Te1	10.4(3)	10.4(3)	15.7(4)	0	0	5.21(16)

Table S4. Bond Lengths from single crystal diffraction of FGaT

Atom	Atom	Length/Å	Atom	Atom	Length/Å
Fe1	$Fe2^1$	2.6581(7)	Fe2	Ga1	2.6581(7)
Fe1	$Fe2^2$	2.6581(7)	Fe2	$Ga1^{10}$	2.6581(7)
Fe1	$Fe2^3$	2.6581(7)	Fe2	$Ga1^{11}$	2.6581(7)
Fe1	$Fe2^4$	2.6581(7)	Fe2	$Te1^1$	2.6979(8)
Fe1	$Fe2^5$	2.6581(7)	Fe2	$Te1^4$	2.6979(8)
Fe1	$Fe2^6$	2.6581(7)	Fe2	$Te1^2$	2.6979(8)
Fe1	$Ga1^1$	2.35121(17)	Fe3	Te1	2.7678(4)

Fe1	Ga1^{2}	2.35118(18)	Fe3	Te1^{1}	2.7678(4)
Fe1	Ga1^{7}	2.35121(17)	Fe3	Te1^{11}	2.7678(4)
Fe1	Te1	2.5629(8)	Fe3	Te1^{4}	2.7678(4)
Fe1	Te1^{8}	2.5629(8)	Fe3	Te1^{10}	2.7678(4)
Fe2	Fe2^{9}	2.480(3)	Fe3	Te1^{2}	2.7678(4)
Fe2	Fe3	2.7834(15)			

^{1}-X,1-Y,1-Z; ^{2}1-X,1-Y,1-Z; ^{3}-X,-Y,1/2+Z; ^{4}-X,-Y,1-Z; ^{5}1-X,1-Y,1/2+Z; ^{6}-X,1-Y,1/2+Z; ^{7}1-X,2-Y,1-Z; ^{8}+X,+Y,3/2-Z; ^{9}+X,+Y,1/2-Z; ^{10}+X,-1+Y,+Z; ^{11}-1+X,-1+Y,+Z

Table S5. Bond Angles from single crystal diffraction of FGaT

Atom	**Atom**	**Atom**	**Angle/°**	**Atom**	**Atom**	**Atom**	**Angle/°**
Fe2^{1}	Fe1	Fe2^{2}	55.61(6)	Ga1^{10}	Fe2	Te1^{5}	80.985(10)
Fe2^{3}	Fe1	Fe2^{4}	55.61(6)	Ga1^{9}	Fe2	Te1^{5}	178.44(6)
Fe2^{3}	Fe1	Fe2^{5}	100.00(4)	Ga1^{9}	Fe2	Te1^{3}	80.984(10)
Fe2^{1}	Fe1	Fe2^{3}	100.00(4)	Ga1^{9}	Fe2	Te1^{1}	80.985(10)
Fe2^{1}	Fe1	Fe2^{5}	100.00(4)	Ga1	Fe2	Te1^{5}	80.984(10)
Fe2^{2}	Fe1	Fe2^{3}	127.501(16)	Ga1^{10}	Fe2	Te1^{1}	178.44(6)
Fe2^{2}	Fe1	Fe2^{4}	100.00(4)	Te1^{5}	Fe2	Fe3	60.63(3)
Fe2^{4}	Fe1	Fe2^{5}	127.501(15)	Te1^{1}	Fe2	Fe3	60.63(3)
Fe2^{6}	Fe1	Fe2^{4}	100.00(4)	Te1^{3}	Fe2	Fe3	60.63(3)
Fe2^{2}	Fe1	Fe2^{6}	100.00(4)	Te1^{5}	Fe2	Te1^{3}	98.01(4)
Fe2^{2}	Fe1	Fe2^{5}	127.501(16)	Te1^{5}	Fe2	Te1^{1}	98.00(4)
Fe2^{3}	Fe1	Fe2^{6}	127.501(15)	Te1^{3}	Fe2	Te1^{1}	98.00(4)
Fe2^{6}	Fe1	Fe2^{5}	55.61(6)	Fe2^{3}	Fe3	Fe2	180.0
Fe2^{1}	Fe1	Fe2^{4}	127.501(16)	Te1^{3}	Fe3	Fe2^{3}	121.844(14)
Fe2^{1}	Fe1	Fe2^{6}	127.501(16)	Te1^{3}	Fe3	Fe2	58.156(14)
Ga1^{5}	Fe1	Fe2^{2}	152.20(3)	Te1^{5}	Fe3	Fe2^{3}	121.844(14)
Ga1^{7}	Fe1	Fe2^{6}	63.751(8)	Te1^{10}	Fe3	Fe2	121.844(14)
Ga1^{1}	Fe1	Fe2^{1}	63.750(8)	Te1^{9}	Fe3	Fe2^{3}	58.156(14)
Ga1^{1}	Fe1	Fe2^{2}	63.750(8)	Te1^{5}	Fe3	Fe2	58.156(14)
Ga1^{1}	Fe1	Fe2^{5}	152.20(3)	Te1^{1}	Fe3	Fe2^{3}	121.844(14)
Ga1^{7}	Fe1	Fe2^{2}	63.750(8)	Te1^{1}	Fe3	Fe2	58.156(14)
Ga1^{5}	Fe1	Fe2^{6}	63.751(8)	Te1^{10}	Fe3	Fe2^{3}	58.156(14)
Ga1^{1}	Fe1	Fe2^{4}	63.751(8)	Te1	Fe3	Fe2^{3}	58.156(14)
Ga1^{5}	Fe1	Fe2^{5}	63.751(8)	Te1	Fe3	Fe2	121.844(14)
Ga1^{7}	Fe1	Fe2^{4}	152.20(3)	Te1^{9}	Fe3	Fe2	121.844(14)
Ga1^{7}	Fe1	Fe2^{5}	63.751(8)	Te1^{9}	Fe3	Te1^{10}	94.728(19)
Ga1^{5}	Fe1	Fe2^{1}	152.20(3)	Te1^{5}	Fe3	Te1^{10}	85.272(19)
Ga1^{7}	Fe1	Fe2^{1}	63.750(8)	Te1	Fe3	Te1^{10}	94.729(19)
Ga1^{5}	Fe1	Fe2^{3}	63.751(8)	Te1^{1}	Fe3	Te1^{10}	180.00(3)
Ga1^{1}	Fe1	Fe2^{6}	152.20(3)	Te1^{5}	Fe3	Te1^{1}	94.728(19)
Ga1^{1}	Fe1	Fe2^{3}	63.751(8)	Te1	Fe3	Te1^{3}	180.0
Ga1^{7}	Fe1	Fe2^{3}	152.20(3)	Te1^{5}	Fe3	Te1^{9}	180.0

Ga1^{5}	Fe1	Fe2^{4}	63.751(8)	Te1	Fe3	Te1^{5}	85.271(19)
Ga1^{5}	Fe1	Ga1^{1}	120.0	Te1^{3}	Fe3	Te1^{1}	94.728(19)
Ga1^{1}	Fe1	Ga1^{7}	120.0	Te1^{3}	Fe3	Te1^{5}	94.729(19)
Ga1^{5}	Fe1	Ga1^{7}	120.0	Te1^{9}	Fe3	Te1^{1}	85.272(19)
Ga1^{1}	Fe1	Te1^{8}	90.0	Te1	Fe3	Te1^{9}	94.729(19)
Ga1^{5}	Fe1	Te1^{8}	90.000(1)	Te1^{3}	Fe3	Te1^{10}	85.272(19)
Ga1^{1}	Fe1	Te1	90.0	Te1^{3}	Fe3	Te1^{9}	85.271(19)
Ga1^{7}	Fe1	Te1^{8}	90.0	Te1	Fe3	Te1^{1}	85.271(19)
Ga1^{5}	Fe1	Te1	90.0	Fe1^{5}	Ga1	Fe1^{7}	120.0
Ga1^{7}	Fe1	Te1	90.0	Fe1^{5}	Ga1	Fe1^{1}	120.0
Te1^{8}	Fe1	Fe2^{6}	62.20(3)	Fe1^{1}	Ga1	Fe1^{7}	120.0
Te1^{8}	Fe1	Fe2^{1}	117.80(3)	Fe1^{1}	Ga1	Fe2	63.751(8)
Te1	Fe1	Fe2^{4}	117.80(3)	Fe1^{1}	Ga1	Fe2^{11}	63.751(8)
Te1^{8}	Fe1	Fe2^{3}	117.80(3)	Fe1^{1}	Ga1	Fe2^{12}	152.20(3)
Te1	Fe1	Fe2^{2}	117.80(3)	Fe1^{7}	Ga1	Fe2	152.20(3)
Te1	Fe1	Fe2^{3}	62.20(3)	Fe1^{1}	Ga1	Fe2^{13}	152.20(3)
Te1^{8}	Fe1	Fe2^{2}	62.20(3)	Fe1^{5}	Ga1	Fe2^{14}	152.20(3)
Te1^{8}	Fe1	Fe2^{4}	62.20(3)	Fe1^{5}	Ga1	Fe2^{13}	63.751(8)
Te1	Fe1	Fe2^{6}	117.80(3)	Fe1^{1}	Ga1	Fe2^{14}	63.750(8)
Te1^{8}	Fe1	Fe2^{5}	117.80(3)	Fe1^{7}	Ga1	Fe2^{11}	152.20(3)
Te1	Fe1	Fe2^{5}	62.20(3)	Fe1^{7}	Ga1	Fe2^{14}	63.750(8)
Te1	Fe1	Fe2^{1}	62.20(3)	Fe1^{5}	Ga1	Fe2^{12}	63.751(8)
Te1^{8}	Fe1	Te1	180.0	Fe1^{1}	Ga1	Fe2^{15}	63.750(8)
Fe1^{5}	Fe2	Fe1^{1}	100.00(4)	Fe1^{7}	Ga1	Fe2^{12}	63.751(8)
Fe1^{3}	Fe2	Fe1^{5}	100.00(4)	Fe1^{7}	Ga1	Fe2^{15}	63.750(8)
Fe1^{3}	Fe2	Fe1^{1}	100.00(4)	Fe1^{7}	Ga1	Fe2^{13}	63.751(8)
Fe1^{5}	Fe2	Fe3	117.80(3)	Fe1^{5}	Ga1	Fe2^{11}	63.751(8)
Fe1^{1}	Fe2	Fe3	117.80(3)	Fe1^{5}	Ga1	Fe2	63.751(8)
Fe1^{3}	Fe2	Fe3	117.80(3)	Fe1^{5}	Ga1	Fe2^{15}	152.20(3)
Fe1^{3}	Fe2	Ga1^{9}	52.498(15)	Fe2^{12}	Ga1	Fe2^{13}	55.61(6)
Fe1^{3}	Fe2	Ga1	124.39(6)	Fe2^{14}	Ga1	Fe2^{15}	55.61(6)
Fe1^{3}	Fe2	Ga1^{10}	52.499(15)	Fe2^{11}	Ga1	Fe2^{13}	100.00(4)
Fe1^{5}	Fe2	Ga1^{10}	52.499(15)	Fe2	Ga1	Fe2^{15}	100.00(4)
Fe1^{5}	Fe2	Ga1	52.498(15)	Fe2^{14}	Ga1	Fe2^{13}	100.00(4)
Fe1^{5}	Fe2	Te1^{1}	127.892(4)	Fe2	Ga1	Fe2^{12}	100.00(4)
Fe1^{1}	Fe2	Te1^{5}	127.892(4)	Fe2^{14}	Ga1	Fe2^{11}	100.00(4)
Fe1^{3}	Fe2	Te1^{1}	127.892(4)	Fe2^{14}	Ga1	Fe2^{12}	127.501(15)
Fe1^{5}	Fe2	Te1^{5}	57.171(16)	Fe2	Ga1	Fe2^{13}	127.501(15)
Fe1^{1}	Fe2	Te1^{3}	127.892(5)	Fe2^{15}	Ga1	Fe2^{12}	100.00(4)
Fe1^{3}	Fe2	Te1^{3}	57.171(16)	Fe2^{15}	Ga1	Fe2^{13}	127.501(15)
Fe1^{5}	Fe2	Te1^{3}	127.893(4)	Fe2^{11}	Ga1	Fe2^{12}	127.501(15)
Fe1^{3}	Fe2	Te1^{5}	127.893(4)	Fe2	Ga1	Fe2^{14}	127.501(15)
Fe1^{1}	Fe2	Te1^{1}	57.170(16)	Fe2	Ga1	Fe2^{11}	55.61(6)
Fe2^{11}	Fe2	Fe1^{5}	62.20(3)	Fe2^{15}	Ga1	Fe2^{11}	127.501(15)
Fe2^{11}	Fe2	Fe1^{1}	62.20(3)	Fe1	Te1	Fe2^{1}	60.63(3)

Fe2[11]	Fe2	Fe1[3]	62.20(3)	Fe1	Te1	Fe2[5]	60.63(3)
Fe2[11]	Fe2	Fe3	180.0	Fe1	Te1	Fe2[3]	60.63(3)
Fe2[11]	Fe2	Ga1	62.20(3)	Fe1	Te1	Fe3[15]	121.844(14)
Fe2[11]	Fe2	Ga1[10]	62.20(3)	Fe1	Te1	Fe3[12]	121.844(14)
Fe2[11]	Fe2	Ga1[9]	62.20(3)	Fe1	Te1	Fe3	121.844(14)
Fe2[11]	Fe2	Te1[3]	119.37(3)	Fe2[1]	Te1	Fe2[5]	98.00(4)
Fe2[11]	Fe2	Te1[5]	119.37(3)	Fe2[1]	Te1	Fe2[3]	98.00(4)
Fe2[11]	Fe2	Te1[1]	119.37(3)	Fe2[5]	Te1	Fe2[3]	98.00(4)
Ga1	Fe2	Fe1[1]	52.499(15)	Fe2[1]	Te1	Fe3[15]	61.21(3)
Ga1[9]	Fe2	Fe1[1]	52.499(15)	Fe2[3]	Te1	Fe3[12]	128.969(9)
Ga1[10]	Fe2	Fe1[1]	124.39(6)	Fe2[1]	Te1	Fe3[12]	128.969(9)
Ga1[9]	Fe2	Fe1[5]	124.39(6)	Fe2[5]	Te1	Fe3[15]	128.969(9)
Ga1[10]	Fe2	Fe3	117.80(3)	Fe2[3]	Te1	Fe3[15]	128.969(9)
Ga1	Fe2	Fe3	117.80(3)	Fe2[5]	Te1	Fe3[12]	61.21(3)
Ga1[9]	Fe2	Fe3	117.80(3)	Fe2[1]	Te1	Fe3	128.969(9)
Ga1	Fe2	Ga1[10]	100.00(4)	Fe2[5]	Te1	Fe3	128.969(9)
Ga1[9]	Fe2	Ga1	100.00(4)	Fe2[3]	Te1	Fe3	61.21(3)
Ga1[9]	Fe2	Ga1[10]	100.00(4)	Fe3[15]	Te1	Fe3	94.730(19)
Ga1[10]	Fe2	Te1[3]	80.985(10)	Fe3	Te1	Fe3[12]	94.730(19)
Ga1	Fe2	Te1[3]	178.44(6)	Fe3[15]	Te1	Fe3[12]	94.730(19)
Ga1	Fe2	Te1[1]	80.984(10)				

[1]-X,1-Y,1-Z; [2]-X,1-Y,1/2+Z; [3]-X,-Y,1-Z; [4]-X,-Y,1/2+Z; [5]1-X,1-Y,1-Z; [6]1-X,1-Y,1/2+Z; [7]1-X,2-Y,1-Z; [8]+X,+Y,3/2-Z; [9]-1+X,-1+Y,+Z; [10]+X,-1+Y,+Z; [11]+X,+Y,1/2-Z; [12]1+X,1+Y,+Z; [13]1+X,1+Y,1/2-Z; [14]+X,1+Y,1/2-Z; [15]+X,1+Y,+Z

Table S6. Space group symmetry determination. Row **N** lists the number of reflections observed that do not exhibit a certain symmetry element. Columns 6_1, 6_2, and 6_3 refer to screw axis symmetry elements and is determined by the (00L) reflections. -c- and --c refers to direction of the mirror plane that is coupled with the translation to the c -axis to form a glide plane aligned to the c-axis. These symmetry elements are determined by the (HHL) reflections. Since the 6_3 and --c symmetry elements have the least number of reflections that do not exhibit those symmetry elements the space group is implied to be *P6₃/mmc*.

	$6_1 = 6_5$	**$6_2 = 3_1$**	**6_3**	**-c-**	**--c**
N	58	49	30	564	244
N I >3σ	34	30	8	434	38
<I>	15.2	17.9	0.2	27.3	0.2
<I/σ>	10.8	12.3	2.0	16.4	1.6

N = No. of Reflections; I = Intensity; σ = error

III. Neutron Powder Diffraction Results

For our Rietveld refinement this general approach was used. First a Le Bail fit was performed to calculate the initial lattice parameters and background fit for each experiment. The Le Bail fit was then used to model any possible micro strain exhibited from the crystal domains. These initial values were then used in the subsequent Rietveld refinement. From this point the first parameter refined was the phase weight of the main FGaT and impure FeTe phases, followed by preferred orientation, then atomic positions, and later isotropic atomic displacement parameters. Fe 1 and Fe 3 were forced to have equivalent U_{iso}. Afterwards, occupancies were then refined flowed by a refinement involving all the variables until convergence was achieved.

For the measurements at or under 323 K. Atomic positions and occupancies were fixed to values used at 348 K. For obtaining magnetic space groups the k-SUBGROUPMAG function from the Bilbao crystal server was used [15].

Table S7. Temperature Dependence of Magnetic Moments Results from Combined Bank 2,4, and 6 Rietveld Refinement

Temperature (K)	**Fe1(μ_B)**	**Fe2(μ_B)**	**Fe3(μ_B)**	***w*R$_p$**
1.5 K	0.73(18)	1.65(6)	-1.61(61)	3.2
150 K	0.66(20)	1.40(6)	-1.48(60)	3.4
298 K	0.57(38)	0.84(12)	-1.67(1.11)	7.4
323 K	0.48(28)	0.64(13)	-3.18(1.38)	7.1

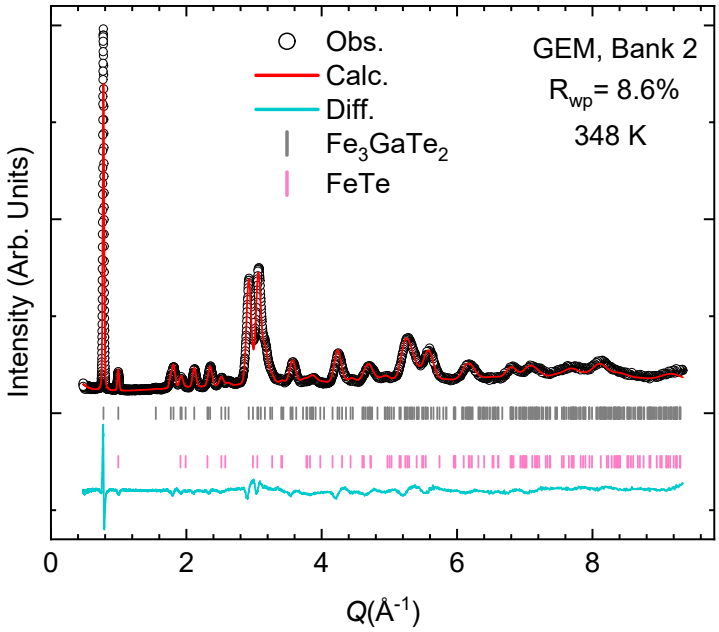

Figure S2. Rietveld refinement of FGaT NPD pattern at 348K. Bank 2

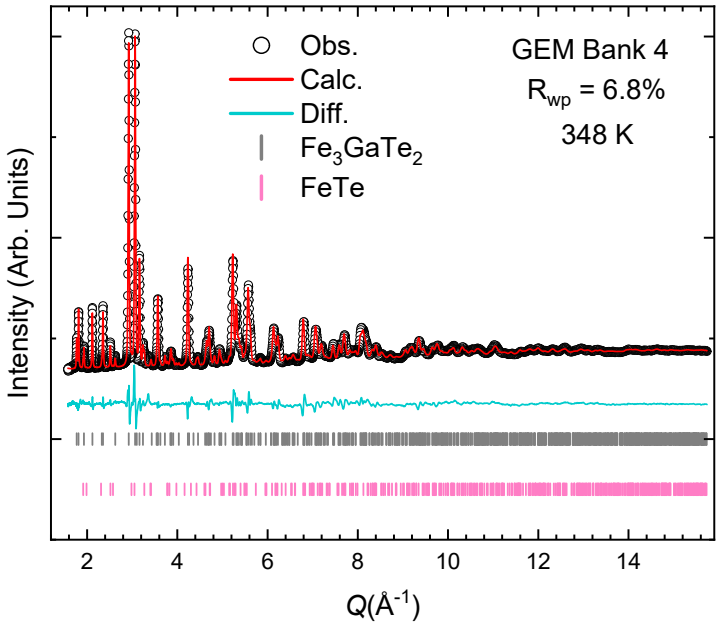

Figure S3. Rietveld refinement of FGaT NPD pattern at 348K. Bank 4

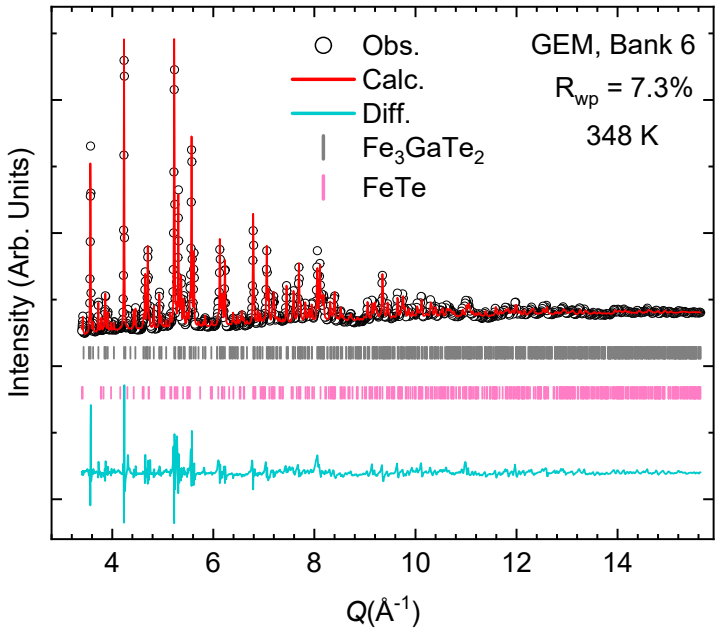

Figure S4. Rietveld Refinement of FGaT with bank 6 data at 348K

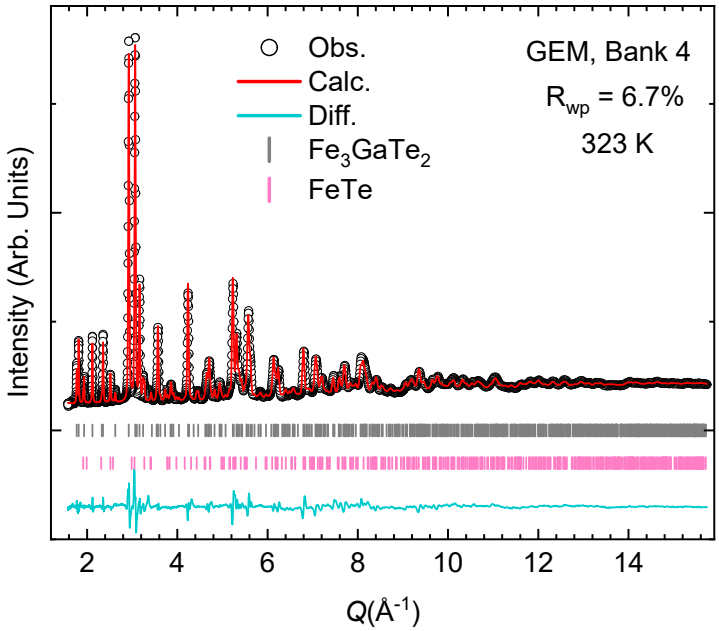

Figure S5. Magnetic Rietveld Refinement of FGaT at 323 K with bank 4 data.

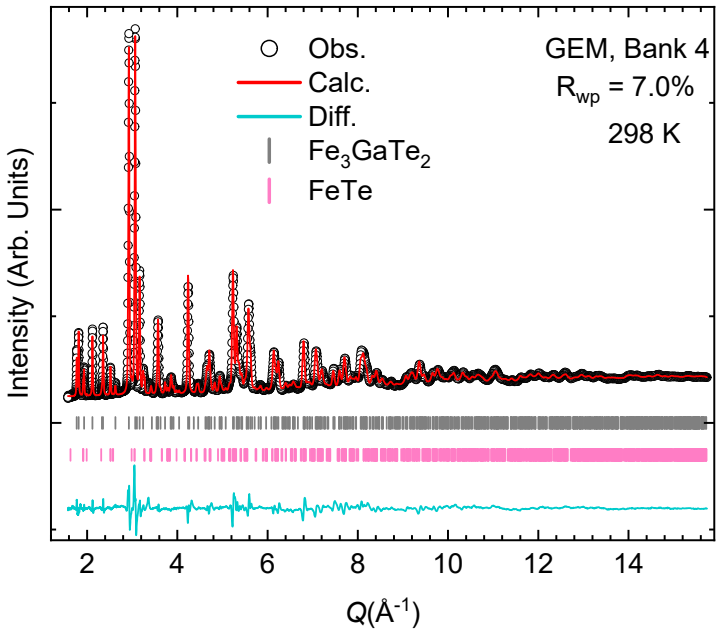

Figure S6. Magnetic Rietveld Refinement of FGaT at 298 K with Bank 4 data

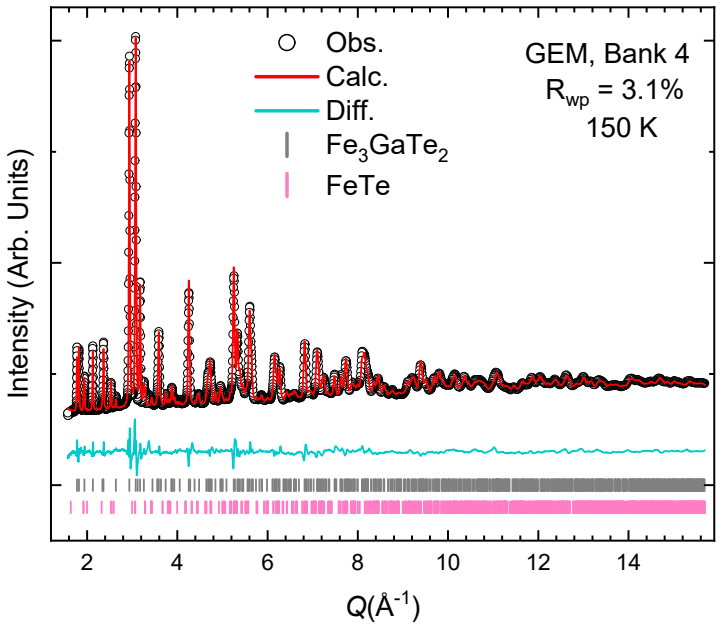

Figure S7. Magnetic Rietveld Refinement of FGaT at 150 K with Bank 4 data

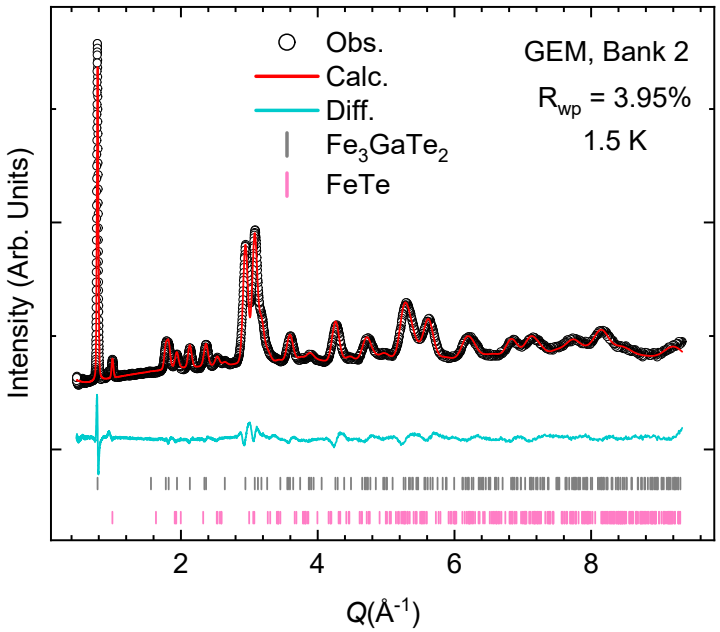

Figure S8. Magnetic Rietveld Refinement of FGaT at 1.5 K with Bank 2 data

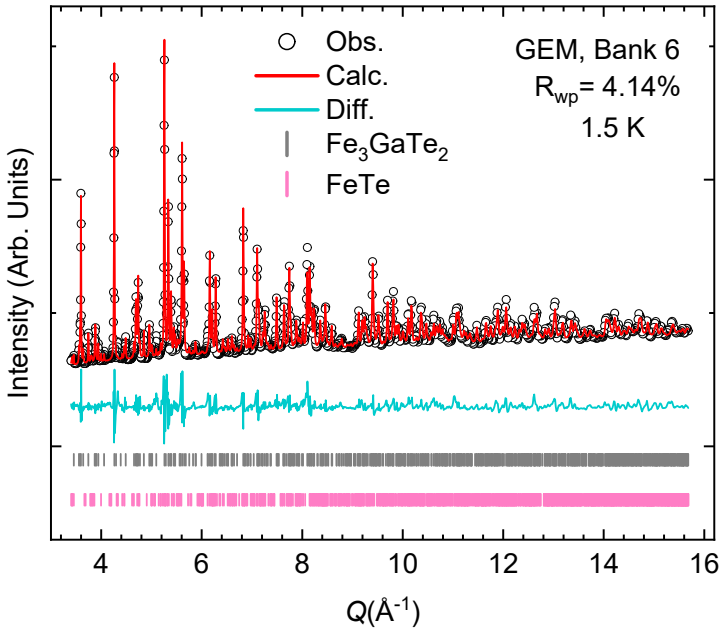

Figure S9. Magnetic Rietveld Refinement of FGaT at 1.5 K with Bank 6 data

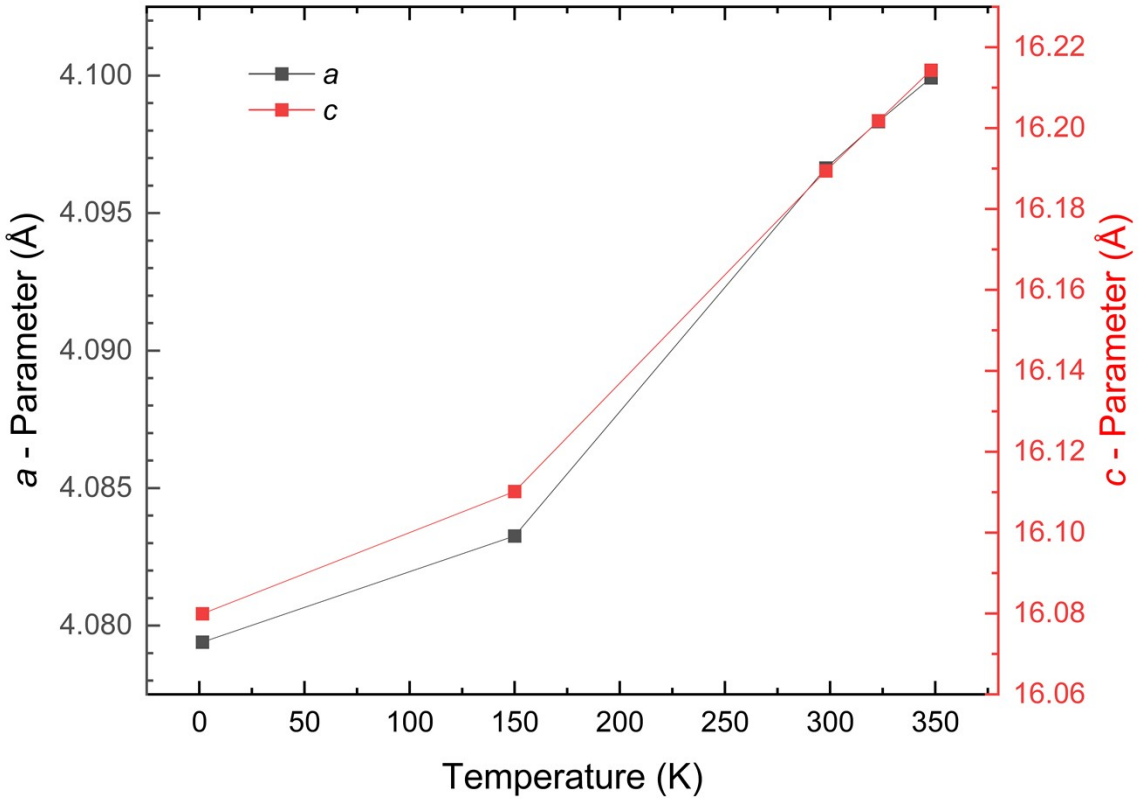

Figure S10. Unit cell parameters *a* and *c* plotted against temperature. Overall, the net effect temperature has on Fe_3GaTe_2 is that it contracts the compound's unit cell. The slight loss in linearity from the data points could be contributed to the change from the ambient to the cryogenic environment at the GEM instrument.

IV. Magnetization and Magnetic Susceptibility

Polycrystalline FGaT was measured with a Microsense© EZ 7 vibrating sample magnetometer. Magnetic susceptibility measurements were performed from 300 K to 450 K with the field at 1000 Oe. Additional magnetic susceptibility measurements were performed utilizing a Quantum Design MPMS©3 SQUID from 2.5 K to 300K with ZFC and FC at 100 Oe of applied magnetic field. Magnetization measurements were performed on FGaT at 300, 330, 350, and 380 K with an applied magnetic field from -20 to 20 kOe with a Microsense© EZ 7 VSM.

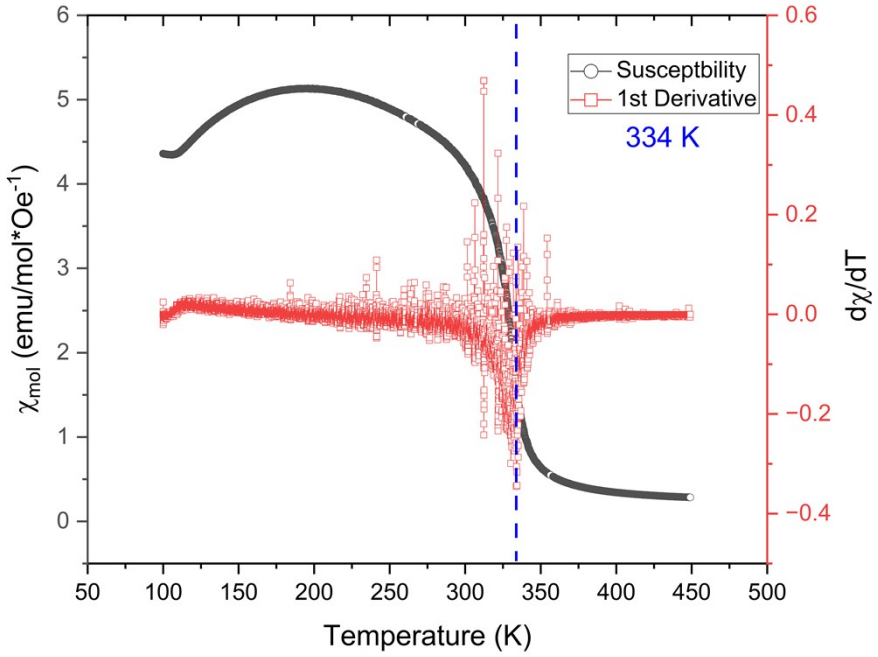

Figure S11. Powder magnetic susceptibility curve and its 1st derivative of polycrystalline Fe_3GaTe_2. Ferromagnetic-like behavior was observed near 334 K.

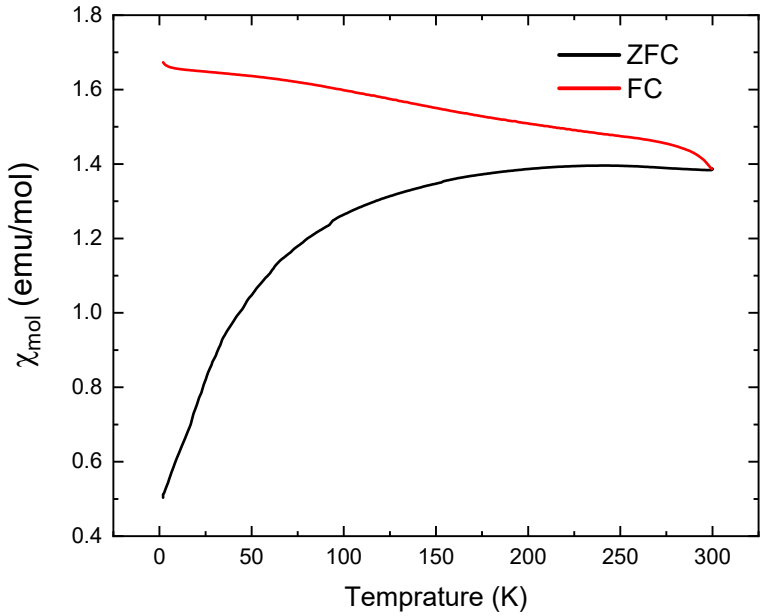

Figure S12. Powder magnetic susceptibility of polycrystalline FGaT using SQUID. ZFC and FC splitting as saturation was observed. These observations are indicative of ferromagnetic behavior.

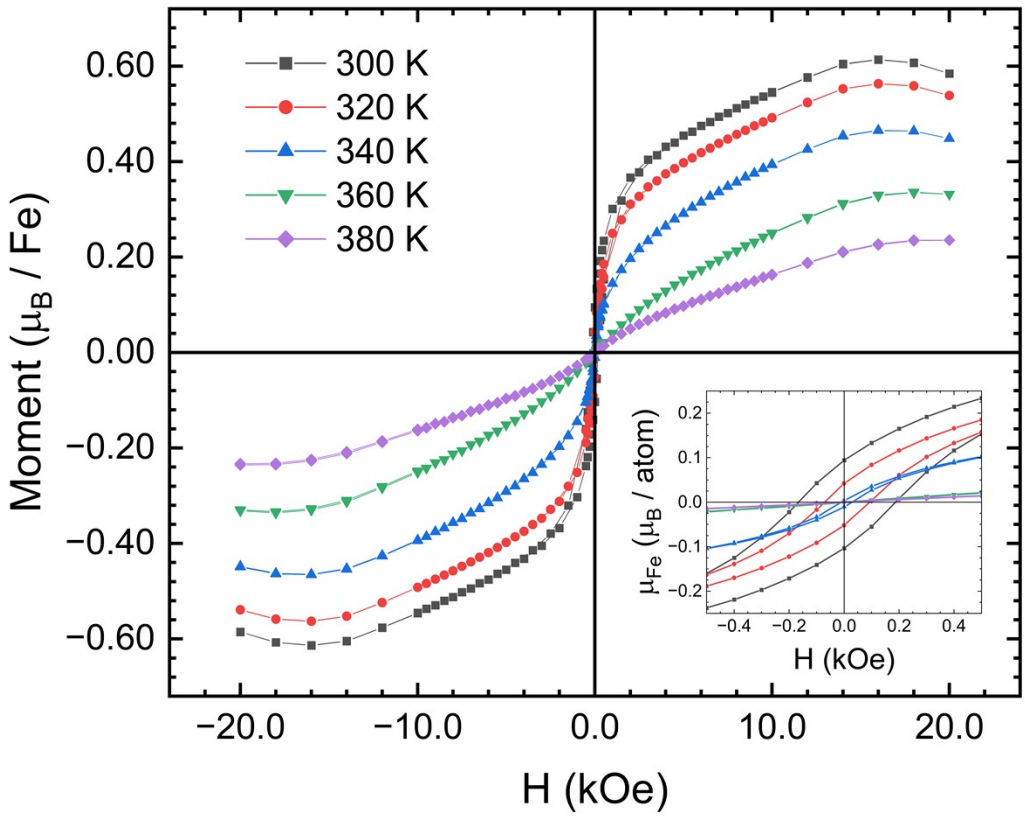

Figure S13. M vs. H curve of polycrystalline Fe_3GaTe_2. M_{sat} at 300 K is near 0.61 μ_B/Fe. This value is less than the reported value of 1.18 μ_B/Fe from Zhang *et.al.* [1] and our the total magnetic moment extracted from our 298 K neutron diffraction results.

V. Density Functional Theory Calculations

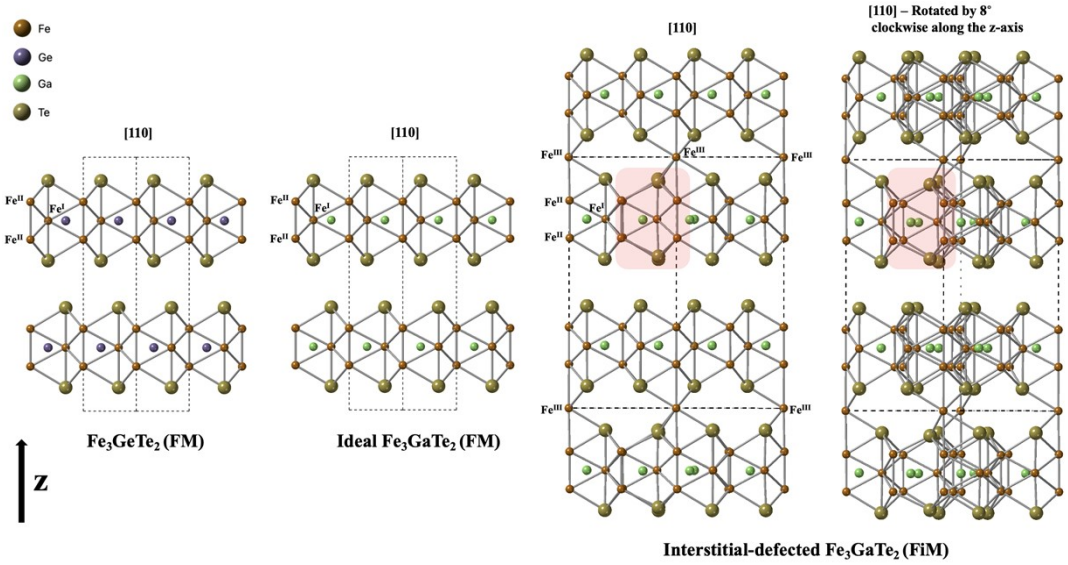

Figure S13. DFT-optimized crystal structures of Fe_3GeTe_2 (from ICSD entry 415616 [16]), ideal Fe_3GaTe_2 (the Ga-substituted version of Fe_3GeTe_2), and Fe_3GeTe_2 with interstitial defects (based on experimental data from XRD). For the interstitial-defected Fe_3GaTe_2, both the original [110] face and the rotated version (rotated by 8° clockwise along the z-axis) are shown to clearly highlight the absence of Fe^I in the cage and the resulting distortion, highlighted by a pink rectangle.

Figure S13 presents the DFT-optimized crystal structures of Fe_3GeTe_2 (FGeT), ideal Fe_3GaTe_2 (FGaT), and interstitial-defect Fe_3GaTe_2 (d-FGaT) structure. The Fe_3GeTe_2 structure was modeled based on ICSD entry 415616 [16]. The ideal Fe_3GaTe_2 was obtained by substituting Ga for Ge in the Fe_3GeTe_2 structure, using the same atomic coordinates and lattice parameters as the starting point for relaxation calculations. The interstitial defect d-FGaT was constructed to reference to experimental data. A 2 × 2 × 1 supercell was employed for d-FGaT to model the partial occupancies of Fe^I (88.5%) and Fe^{III} (12.5%), with Fe^{III} occupying an interstitial site between adjacent double layers. Specifically, atomic coordinates derived from XRD data were used to generate a 2 × 2 × 1 supercell in the hexagonal crystal system (space group No. 194, $P6_3/mmc$). One of the eight Fe^I atoms was then moved into an interstitial position to simulate a partial occupancy of Fe^I (88.5%) and Fe^{III} (12.5%), comparable to the vacancy observed in experiment. The removal of Fe^I atom creates a hole at the center of the cage, and with the introduction of interstitial Fe^{III} into the vdW gap, causes a slight distortion of bond lengths, and is highlighted by the pink rectangle in **Figure S13**.

Table S8. Comparison of the moment size for different magnetic orders from DFT calculations and neutron diffraction results. The models include ferromagnetic (FM) Fe3GeTe2 (FGT), ferromagnetic Fe3GaTe2 (FGaT) with only 2 sites and ferrimagnetic (FiM) with the interstitial site added (3-site). The experimental values from neutron diffraction are included for comparison.

Material	**FGT**	**FGaT**	**FGaT**	**FGaT**
Model	DFT	2-sites (DFT)	3-sites (DFT)	Exp.
Magetic state	FM	FM	FiM	FiM
Magnetic Moment (μ_B)				
- Fe1 (Avg.)	1.54	1.54	1.68	0.73(18)
- Fe2 (Avg.)	2.39	2.35	2.32	1.65(6)
- Fe3 (Avg.)	-	-	-2.82	-1.6(6)
Total Magnetization (μ_B/cell)	12.53	12.11	11.18	-
Absolute Magnetization (μ_B/cell)	14.10	13.99	14.30	-

VI. References

[1] Zhang, G., Guo, F., Wu, H. *et al.* Above-room-temperature strong intrinsic ferromagnetism in 2D van der Waals Fe_3GaTe_2 with large perpendicular magnetic anisotropy. *Nat Commun*, **2022**, 13, 5067.

[2] Bruker (2021). Apex4. Bruker AXS Inc., Madison, Wisconsin, USA.

[3] Krause, L., Herbst-Irmer, R., Sheldrick, G.M., Stalke, D. *J. Appl. Cryst*. **2015**, 48, 3-10.

[4] Sheldrick, G. M. *Acta Cryst*. **2015**, A17, 3-8.

[5] Sheldrick, G. M. *Acta Cryst*. **2015**, C17, 3-8.

[6] Toby, B. H. & Von Dreele, R. B. GSAS-II: the genesis of a modern open-source all purpose crystallography software package. *J. Appl. Cryst*. 46, 544-549, 2013.

[7] P. Giannozzi, S. Baroni, N. Bonini, M. Calandra, R. Car, C. Cavazzoni, D. Ceresoli, G.L. Chiarotti, M. Cococcioni, I. Dabo, QUANTUM ESPRESSO: a modular and open-source software project for quantum simulations of materials, *J. Phys.: Condens. Matter*. **2009**, 21, 395502.

[8] P. Hohenberg, W. Kohn, Inhomogeneous electron gas, *Physical Review.* **1964**, 136, B864.

[9] W. Kohn, L.J. Sham, Self-consistent equations including exchange and correlation effects, *Physical Review,* **1965**, 140, A1133.

[10] W. Kohn, L.J. Sham, Quantum density oscillations in an inhomogeneous electron gas, *Physical Review*. **1965**, 137, A1697.

[11] J.P. Perdew, K. Burke, M. Ernzerhof, Generalized gradient approximation made simple, *Physical Review Letters.* **1996,** 77, 3865.

12] S. Grimme, Semiempirical GGA-type density functional constructed with a long-range dispersion correction, *J. Comput. Chem.* **2006**, 27, 1787–1799.

[13] K.F. Garrity, J.W. Bennett, K.M. Rabe, D. Vanderbilt, Pseudopotentials for high-throughput DFT calculations, *Comput. Mater. Sci.* **2014**, 81, 446–452.

[14] H.J. Monkhorst, J.D. Pack, Special points for Brillouin-zone integrations, *Phys. Rev. B*. **1976**, 13, 5188–5192.

[15] J.M. Perez-Mato, S.V. Gallego, E.S. Tasci, L. Elcoro, G. de la Flor, and M.I. Aroyo "Symmetry-Based Computational Tools for Magnetic Crystallography" *Annu. Rev. Mater. Res.* **2015**, 45:13.1-13.32.

[16] H.-J. Deiseroth, K. Aleksandrov, C. Reiner, L. Kienle, R.K. Kremer, Fe3GeTe2 and Ni3GeTe2–two new layered transition-metal compounds: crystal structures, HRTEM investigations, and magnetic and electrical properties, *Wiley Online Library*, **2006**.